Available online at www.sciencedirect.com
SCIENCE DIRECT®
Journal of Nuclear Materials 337–339 (2005) 45–49
journal of nuclear materials
www.elsevier.com/locate/jnucmat

Simulation study on influence of chemically eroded higher hydrocarbons on SOL impurity transport and effect of dynamical material mixing on erosion/deposition of tungsten surfaces exposed to boundary plasmas

R. Kawakami *, T. Mitani

Faculty of Engineering, The University of Tokushima, Tokushima 770-8506, Japan

Abstract

Local transport of CD and C^+ generated through the reaction chains of CD_4, C_2D_4 and C_3D_6 chemically eroded from C targets exposed to the boundary plasmas and generated through C^0 emitted from the C targets is simulated. The simulation reproduces the CD and CII emission distributions measured in TEXTOR-94. For CD, there are a strong contribution of C_2D_4 and a weak contribution of C_3D_6 near the target. For CII, contributions of C_2D_4 and C_3D_6 are weak. By changing the C impurity concentration and target temperature, erosion/deposition of W targets exposed near and far from the last close flux surface is also simulated. The near–far asymmetry observed in TEXOR-94, which means erosion of the near target and deposition on the far target, is qualitatively reproduced depending on the plasma parameters, the C impurity concentration and the target temperature.

PACS: 34.50.Dy; 52.25.Vy; 52.40.Hf; 52.65.Pp; 66.30.Jt
Keywords: Carbon impurities; Chemical erosion; Diffusion; Erosion & Deposition; Edge plasma

1. Introduction

For a plasma-facing material in the divertor, C and W are the excellent candidates. In terms of the impurity level, however, transport of hydrocarbon species eroded through chemical reactivity of C with D^+ in the scrape-off layer (SOL) is a crucial issue [1]. The hydrocarbon transport makes the impurity control more difficult. Thus, it is necessary to clarify how the hydrocarbon species influence the impurity transport. From the viewpoint of the target lifetime, material mixing between C and W on a W target exposed to D plasmas including C impurity is also a crucial issue [2]. The previous study showed that the diffusion of C impurity deposited on the W target contributes to the material mixing [3]. Thus, the effect of material mixing resulting from collision and diffusion processes on the erosion/deposition of the W target needs to be cleared up.

In this study, an influence of chemically eroded hydrocarbons, CD_4, C_2D_4 and C_3D_6, on the local transport of C impurities, CD and C^+, in the SOL plasma is investigated using a plasma–surface interaction code, EDDY [4]. Also, effect of the material mixing on

* Corresponding author. Tel./fax: +81 88 656 7441.
E-mail address: retsuo@ee.tokushima-u.ac.jp (R. Kawakami).

0022-3115/$ - see front matter © 2004 Elsevier B.V. All rights reserved.
doi:10.1016/j.jnucmat.2004.08.027

erosion/deposition of W targets during the exposure is investigated by changing the C impurity concentration in the plasma and the target temperature. Emphasis is put on a change in the local transport for different plasma parameters. For the W targets, attention is paid to a dependence of the erosion/deposition upon the plasma parameters, the C impurity concentration and the target temperature. The results are compared with TEXTOR experimental data [2,5].

2. Simulation code for plasma–surface interactions at carbon and tungsten surfaces

EDDY calculates local transport of CD_4, C_2D_4 and C_3D_6 chemically eroded from C targets exposed to the boundary plasmas and that of C^0 emitted from the C targets (reflection plus physical erosion). The local transport is based on the Lorentz force motion, including the ionization and dissociation reactions with e^- and the charge exchange reactions with D^+ in the plasma. The atomic and molecular reactions are modeled to occur according to the reaction rates as a function of electron temperature [6–8]. The emission energy of the hydrocarbons is simply assumed to be the Maxwellian distribution with the target temperature, which is partially justified around the peak [9]. For the atoms, the emission energy is based on the binary collision model [10]. The sticking coefficient of hydrocarbons locally returned back to the targets is assumed to be 0%: the locally returned CD_x ($x = 14$) is re-eroded as CD_4. The assumption is justified by the result: the code reproduces the ^{13}C deposition pattern in the $^{13}CH_4$ gas puffing experiment on TEXTOR [11]. The particle transport is followed until the eroded impurity particle either is redeposited on the targets or leaves the computational domain [4].

Also, EDDY calculates temporal evolution of erosion/deposition of W targets exposed to D plasmas including C impurity, resulting from material mixing between the W target and the deposited C due to the collision and diffusion processes [4]. In the collision process, the C deposition, erosion of the W target and the deposited C, and the resultant composition change in the target are simulated based on the binary collision model [10]. The diffusion process is based on the diffusion equation with the diffusion coefficient $D = D_0 \exp(-Q/k_B T)$, where k_B is the Boltzmann constant and T is the target temperature. In this study, the diffusion coefficient $D_0 = 3.15 \times 10^7$ m^2/s and the activation energy $Q = 1.78$ eV are used for C in W, which were obtained in another diffusion experiment [12]. By using the diffusion coefficient, the EDDY simulation reproduced the measured weight change of a W target by C^+ impact [13] and the measured depth profile of C impurity deposited on a W target exposed to a D^+ plasma including C^{4+} impurity [3]. The temporal evolution of erosion/deposition is calculated by alternately simulating the two processes, which is identical with TRIDYN/PIDAT [14].

3. Results and discussion

3.1. Local transport of higher hydrocarbons chemically eroded from carbon surfaces for different plasma parameters

The simulation for the hydrocarbon transport is based on experimental conditions for a C test limiter exposed to the TEXTOR-94 edge plasmas [15]. The top of the limiter is located at a minor radius of $r \sim 46$ cm, at which there is the last closed flux surface (LCFS) formed by a graphite main limiter. The radial distributions of edge plasma density and temperature fitted exponentially to those measured by the Li- and He-diagnostics are used. The density and temperature at the LCFS are $n_{eLCFS} = 10^{12}$ cm^{-3} and $T_{eLCFS} = 30$ eV, respectively, and their e-folding lengths are $\lambda_{ne} = 2.0$ cm and $\lambda_{Te} = 2.5$ cm, respectively [5,16]. Based on the experimental features, D^+ and C^{4+} are used as plasma ions, assuming $T_i = T_e$ [16].

Assuming that the total chemical erosion yield, $Y_{CHEM} = Y_{CD4} + Y_{C2D4} + Y_{C3D6}$ is $Y_{CHEM} = 0.045$ ($Y_{CD4} = 0.037$, $Y_{C2D4} = 0.007$, $Y_{C3D6} = 0.001$), the behavior of CD and C^+ penetration into the plasma from the C target exposed to the D^+ plasma including C^{4+} impurity is simulated as shown in Fig. 1. The value of Y_{CHEM} is based on the TEXTOR experiment [15]. As a simple model, the three high erosion yields of the C_1-, C_2- and C_3-containing molecules are preferentially chosen, and the yield ratios of Y_{C2D4}/Y_{CD4} and Y_{C3D6}/Y_{CD4} are determined based on 200 eV D^+ beam exposure experiment on graphite at 700 K [1]. As shown in Fig. 1(a), the penetration of CD generated through the CD_4, C_2D_4 and C_3D_6 reaction chains (black thick curves) is in a good agreement with the measured CD light emission distribution [15]. Therefore, the chemical erosion of CD_4 determines the CD penetration at the distance more than ~0.5 cm from the target, whereas the contribution of C_2D_4 dominates near the target. The contribution of C_3D_6 is weak because Y_{C3D6} is low. Therefore, the contribution of C_2D_4 to the CD penetration is not negligible near the target. For C^+ generated through the C^0, CD_4, C_2D_4 and C_3D_6 reaction chains (black thick curve), the measured CII light emission distribution [5] is also reproduced (1(b)). There is a strong contribution of CD_4 at less than ~2.5 cm from the target, and that C^0 dominates further.

If the density increases to $n_{eLCFS} = 10^{13}$ cm^{-3}, the CD and C^+ penetration is significantly suppressed as shown in Fig. 2(a) and (b). The suppression is due to the higher local redeposition: for the high density, the

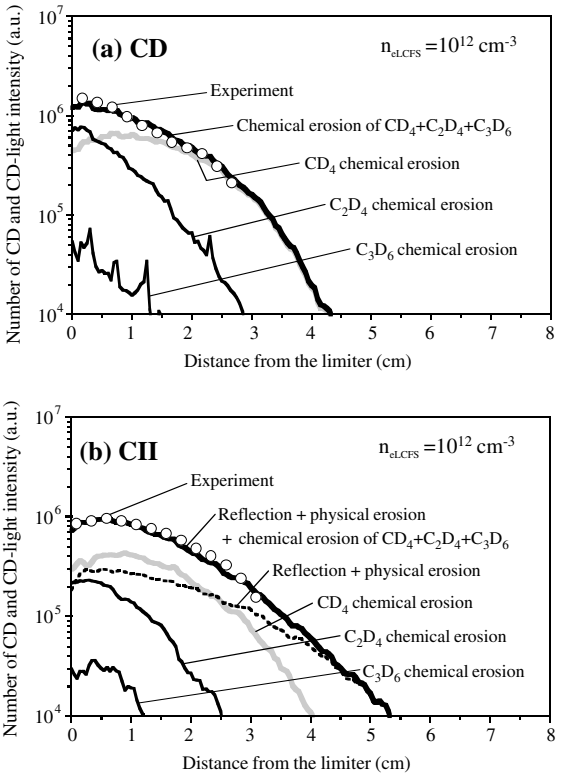

Fig. 1. Radial penetration profiles of (a) CD and (b) C^+ generated through the reaction chains of CD_4, C_2D_4 and C_3D_6 chemically eroded from the C target and generated through those of C^0 emitted from the C target. Open circles in the figures indicate the experimental data of CD and CII light intensities, respectively [5,15].

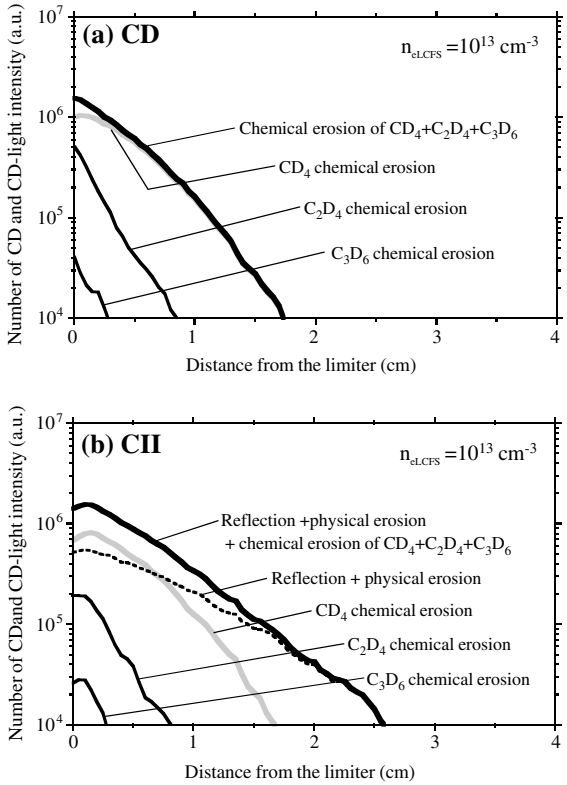

Fig. 2. The same as Fig. 1, but $n_{eLCFS} = 10^{13}\,cm^{-3}$ (no experimental data).

redeposition rates of the hydrocarbons ($R_{CD4} = 17\%$, $R_{C2D4} = 60\%$ and $R_{C3D6} = 78\%$) are higher than those at the low density ($R_{CD4} = 1\%$, $R_{C2D4} = 20\%$ and $R_{C3D6} = 30\%$), respectively. Also, the contributions of the higher hydrocarbons are weakened compared with those of CD_4. Therefore, at the high density, the CD and C^+ penetration is dominated by the contribution of CD_4 and C^0.

However, if the temperature decreases below $T_{eLCFS} = 30$ eV, the result may be different. According to the D^+ exposure experiment, Y_{CD4}, Y_{C2D4} and Y_{C3D6} become lower if the exposure energy decreases, but the yield ratios of Y_{C2D4}/Y_{CD4} and Y_{C3D6}/Y_{CD4} become higher [1]. Also, the local redeposition would hardly occur at the low temperatures, because the reaction rates of C_xD_y with e^- become lower [6–8]. In addition, another study shows that, for a fresh re-deposited layer, the chemical erosion is more enhanced [17]. Therefore, under the detached plasma conditions in the divertor, the contributions of the higher hydrocarbons on the CD and C^+ penetration may be enhanced.

3.2. Erosion/deposition of tungsten surfaces for different carbon impurity concentrations and target temperatures

The simulation for erosion/deposition of the W targets is based on experimental conditions for a 300 nm thick W layer on a graphite sample exposed to the TEXTOR-94 edge plasmas [2]. The target is inclined by 20° to the toroidal magnetic field. For the plasma density and temperature, the exponentially fits are used [2]: $n_{eLCFS} = 10^{12}$ cm^3 ($\lambda_{ne} = 2.55$ cm) and $T_{eLCFS} = 40$ eV ($\lambda_{Te} = 7.5$ cm). In the simulation, the C impurity concentration in the plasma and the target temperature are varied, because their experimental values are uncertain [2,18]. For the simulation, attention is paid to the two W spot targets exposed near and far from the LCFS (at $r = 49.3$ cm and 50.1 cm).

By changing the C impurity concentration and the target temperature, a change in temporal evolution of erosion/deposition of the two targets is simulated as shown in Fig. 3. The C impurity concentration significantly changes the target temperature dependence of the erosion/deposition. For a low C impurity concentration (C:2.0%), with increasing target temperature, there is a transition from erosion to deposition at both the near and far targets (Fig. 3(a) and (b)). Namely, the

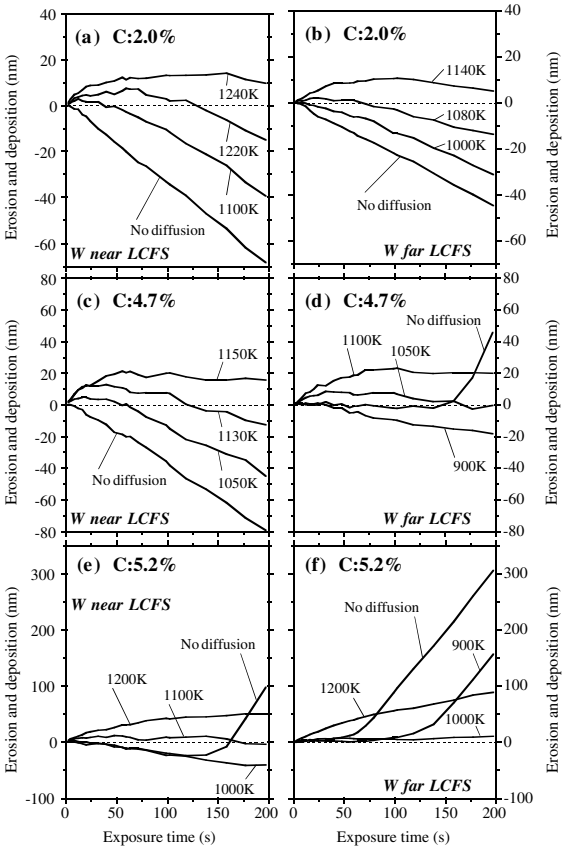

Fig. 3. Temporal evolution of erosion/deposition of the W targets for different C impurity concentrations and target temperatures. On the vertical axis, plus and minus signs show deposition and erosion, respectively.

two targets show the same temperature dependence. The transition is because the deposited C expands deeply by the diffusion, which results in formation of a thick W–C mixed layer (not shown here).

If the C impurity concentration increases to C:4.7%, there is a significant difference in the temperature dependence between the two targets. The near target shows the same temperature dependence as for C:2.0% (Fig. 3(c)). The far target shows a non-monotonic excursion, which means that deposition and erosion occur alternately with increasing target temperature (Fig. 3(d)). The excursion is also found in another simulation study of a W target irradiated with H^+ and C^+ mixed beam [19]. This results from a synergistic effect of the diffusion and the reflective scattering collision from the W–C mixed layer near the surface [20]. Namely, the impinging ions tend to be reflected from the W atoms in the W–C mixed layer formed by the diffusion. The reflected ions knock off the C atoms from the top surface. As a result, erosion of the deposited C is enhanced (compared with that of pure C bulk), which results in the first transition

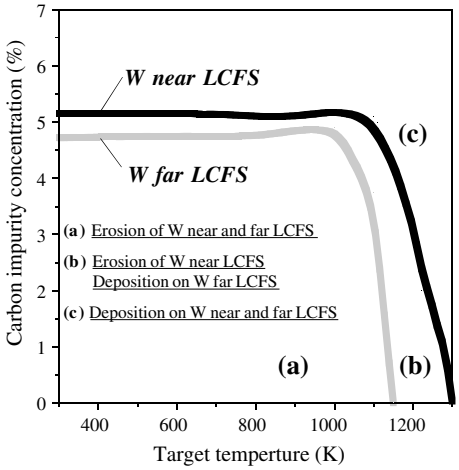

Fig. 4. Dependence of erosion/deposition of the W targets upon the C impurity concentration and the target temperature. Black and gray curves correspond to the critical C impurity concentrations at which a transition from erosion to deposition occurs for the targets near and far from the LCFS, respectively.

from deposition to erosion. The second transition from erosion to deposition results from the same reason as for C:2.0%. For C:5.2%, the different trend occurs. The near target shows the excursion (Fig. 3(e)), whereas the far target shows deposition only, but its amount is changed (Fig. 3(f)). The reason for the deposition only is simply that the deposited C is thick enough not to be eroded.

A relationship of the erosion/deposition of the two targets with the C impurity concentration and the target temperature is summarized in Fig. 4. For the near target, the critical C impurity concentration at which a transition from erosion to deposition occurs decreases with increasing target temperature. For the far target, the same trend occurs, but the critical C impurity concentration is lower. The difference in the critical C impurity concentration between the two targets causes the near–far asymmetry in the erosion/deposition, which means erosion of the near target and deposition on the far target, at the (b) region delimited by the black and gray curves in Fig. 4. For example, even at C:2.0%, the near–far asymmetry is found to occur if the target temperature is high. The results in the (b) region qualitatively reproduce the TEXTOR-94 experimental data [2], which occur depending on the plasma parameters, the C impurity concentration and the target temperature.

4. Conclusion

Radial penetration of CD and C^+ generated through the reaction chains of CD_4, C_2D_4 and C_3D_6 chemically

eroded from C targets and generated through those of C^0 emitted from the C targets have been simulated. The results reproduce the CD and CII emission distributions measured in TEXTOR-94. For CD, there is the strong contribution of C_2D_4 near the target. For CII, the contributions of C_2D_4 and C_3D_6 are weak. If the plasma density increases to $\sim 10^{13}$ cm^{-3}, however, there is little contribution of the higher hydrocarbons to the CD and C^+ penetration, which is dominated by the contribution of CD_4 and C^0.

By changing the C impurity concentration and the target temperature, erosion/deposition of W targets exposed near and far from the LCFS due to the material mixing has been simulated. The results show that the erosion and deposition alternate with increasing target temperature, and that the C impurity concentration changes the target temperature dependence of erosion/deposition. The critical C impurity concentration is also shown to decrease with increasing target temperature. The near–far asymmetry observed in TEXTOR-94 (erosion of the near target and deposition on the far target) is qualitatively reproduced depending on the plasma parameters, the C impurity concentration and the target temperature.

References

[1] B.V. Mech, A.A. Haasz, J.W. Davis, J. Nucl. Mater. 255 (1998) 153.
[2] D. Hildebrandt, P. Wienhold, W. Schneider, J. Nucl. Mater. 290–293 (2001) 89.
[3] R. Kawakami, K. Ohya, J. Nucl. Mater. 313–316 (2003) 107.
[4] R. Kawakami, Jpn. J. Appl. Phys. 43 (2004) 785.
[5] A. Kirschner, V. Philipps, A. Pospieszczyk, P. Wienhold, Phys. Scr. T91 (2001) 57.
[6] M.A. Lennon, K.L. Bell, H.B. Gilbody, J.C. Hughes, A.E. Kingston, M.J. Murray, F.J. Smith, Rep. Culham Lab., CLM-R270, 1986.
[7] A.B. Ehrhardt, W.D. Langer, Rep. Princeton Plasma Phys. Lab., PPPL-2477, 1986.
[8] J.N. Brooks, Z. Wang, D.N. Ruzic, D.A. Alman, Rep. Argonne Natl. Lab. ANL/FPP/TM-297, 1999.
[9] E. Vietzke, J. Nucl. Mater. 290–293 (2001) 158.
[10] W. Möller, W. Eckstein, J.P. Biersack, Comput. Phys. Commun. 51 (1988) 355.
[11] A. Kirschner, A. Huber, V. Philipps, A. Pospieszczyk, P. Wienhold, J. Winter, J. Nucl. Mater. 290–293 (2001) 238.
[12] H. Bakker, H.P. Bonzel, C.M. Bruff, M.A. Dayananda, W. Gust, J. Horváth, I. Kaur, G.V. Kidson, A.D. LeClaire, H. Mehrer, G.E. Murch, G. Neumann, N. Stolica, N.A. Stolwijk, in: H. Mehrer (Ed.), Diffusion in Solid Metals and Alloys, Springer, Berlin, 1990, p. 480.
[13] R. Kawakami, K. Ohya, Jpn. J. Appl. Phys. 42 (2003) 5259.
[14] W. Eckstein, V.I. Shulga, J. Roth, Nucl. Instrum. and Meth. B 153 (1999) 415.
[15] A. Pospieszczyk, V. Philipps, E. Casarotto, U. Kögler, B. Schweer, B. Unterberg, F. Weschenfelder, J. Nucl. Mater. 241–243 (1997) 833.
[16] M. Brix, Report of IPP Jülich, Jül-3638, 1998.
[17] A. Kirschner, P. Wienhold, V. Philipps, J.P. Coad, A. Huber, U. Samm, JET EFDA contributors, J. Nucl. Mater. 328 (2004) 62.
[18] V. Philipps, T. Tanabe, Y. Ueda, A. Pospieszczyk, M.Z. Tokar, B. Unterberg, L. Konen, B. Schweer, U. Samm, P. Wienhold, J. Winter, M. Rubel, B. Emmoth, N.C. Hawkes, the TEXTOR TEAM, Nucl. Fusion 34 (1994) 1417.
[19] R. Kawakami, T. Shimada, Y. Ueda, M. Nishikawa, J. Nucl. Mater. 329–333 (2004) 737.
[20] R. Kawakami, K. Ohya, Jpn. J. Appl. Phys. 40 (2001) 6581.